

In Vivo Detection of Glutamate in Tomatoes by an Enzyme-Based Electrochemical Biosensor

Shunkun Tang, Cheng Wang, Ke Liu, Bin Luo, Hongtu Dong, Xiaodong Wang, Peichen Hou, and Aixue Li*



Cite This: *ACS Omega* 2022, 7, 30535–30542



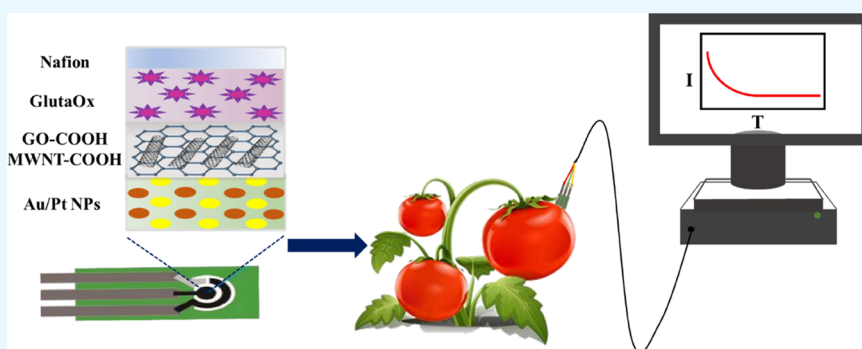
Read Online

ACCESS |

Metrics & More

Article Recommendations

Supporting Information



ABSTRACT: The in vivo and on-site detection of key physiology parameters in plants will be of great relevance for precision agriculture and food technology. In this work, a sensitive enzymatic glutamate sensor was successfully developed. To enhance the conductivity and catalytic ability and to fix the glutamate oxidase, Au–Pt nanoparticles were first deposited on screen-printed electrodes, and then carboxylated graphene oxide and carboxylated multiwalled carbon nanotubes were fabricated for the synthesis of the electrode. The detection range of the glutamate sensor is widest ($2\ \mu\text{M}$ to $16\ \text{mM}$) up to date, and its detection limit is relatively low ($0.14\ \mu\text{M}$). A number of standard curves were built in the pH range of 3.5–7.5, which can be applied in various plants and fruits. Using this sensor, the glutamate level in tomatoes was determined in vivo. This glutamate sensor has important practical value in precision agriculture. Our strategy also provides a way to establish the detection modes for other biomolecules in plants.

1. INTRODUCTION

L-Glutamate is an amino acid which occurs naturally in plants. It plays an important role in protein metabolism, provides energy and materials for plant growth, and promotes the development of plant organs. Glutamate also links nitrogen metabolism^{1,2} with carbon metabolism to produce amino-butyric acid,^{3,4} arginine,⁵ serine, cysteine, and other substances required for plant metabolism, which provides conditions for plant environmental adaptability. In addition, glutamate is an important nutrient in fruits; it is an important indicator for fruit yield and quality. With the development of precision agriculture, researchers hope to monitor the changes of glutamate content in plants in vivo and on site and timely evaluate the growth status of plants and the nutritional level of fruits, so as to realize the precise regulation of agriculture and serve food technology.

Different techniques have been used for detecting glutamate, for example, chromatography,^{6,7} spectrophotometry,^{8,9} fluorimetry,^{10,11} and so on. However, these methods are all used in vitro. The plant samples need to be pretreated. This process is complex and time-consuming, and some important biological information will always be lost during this process. In vivo

techniques for detecting glutamate have also been developed, such as nuclear magnetic resonance spectroscopy,¹² positron emission tomography, and so on. However, these apparatuses are expensive and not portable. They are not adaptable for on-site application in precision agriculture.

Electrochemical sensors are one of the most potential approaches for in vivo and on-site monitoring of biomolecules, because of their simplicity, sensitivity, portability, and easy-to-miniaturize and -integrate nature.^{13–18} Several in vivo electrochemical sensors for glutamate have been developed. For example, for in vivo glutamate monitoring in spinal cord, Nguyen et al. have fabricated a flexible glutamate biosensor using a simple direct ink writing technique.¹⁹ Ganesana et al. developed a microbiosensor for in vivo monitoring of glutamate release in the brain.²⁰ However, these glutamate

Received: June 27, 2022

Accepted: August 4, 2022

Published: August 16, 2022



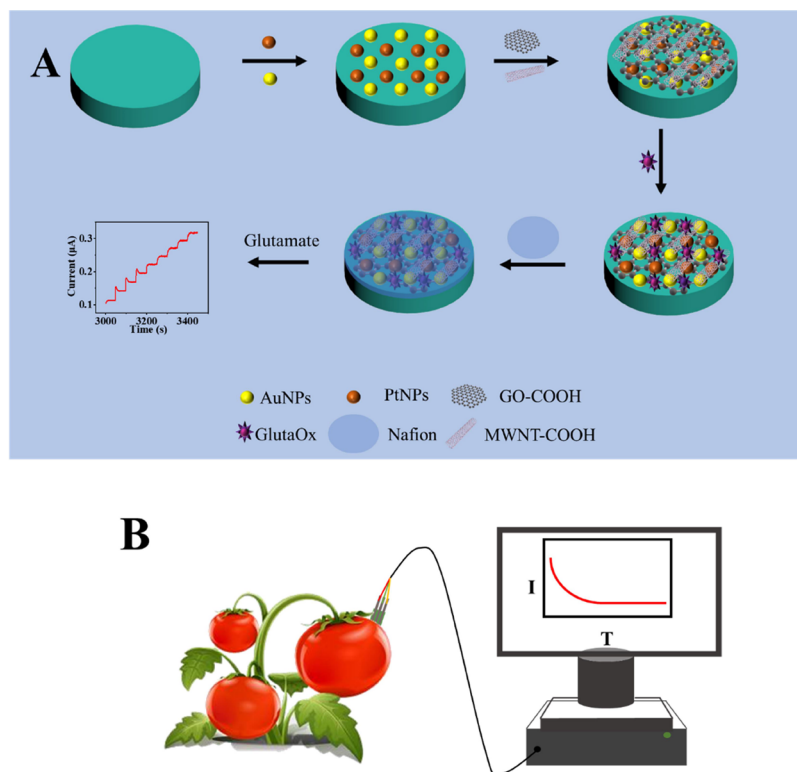


Figure 1. Schematic diagram of the preparation process of the glutamate sensor (A), and schematic illustration of in vivo detection of glutamate in tomato fruits (B).

sensors were developed based on the application in humans or animals. The content of glutamate in plants is much higher than that in animals and humans. For example, the glutamate in watermelon is about 12 mM,²¹ while the glutamate in the extracellular space of the human brain is in the range of 4–350 μM .²² Moreover, the pH of plant juice is quite different from that of blood of animals and humans. Most fruits are acidic. The pH value of plant juice varies greatly according to different species, different growth stages, and different tissue types. Therefore, the developed glutamate sensors are not suitable for plants, and there is an urgent need for developing in vivo and on-site sensors for glutamate in plants.

To develop a practical sensor which can be widely used in agriculture, screen-printed electrodes (SPEs) were applied because of their low cost and mature manufacturing technology. For enzymatic biosensors, the enzyme plays a crucial role in oxidizing and detecting the target molecules. In our work, L-glutamate oxidase (GlutaOx) was used as it does not need the help of coenzymes.²³ Nanomaterials have been widely used in electrochemical biosensors to improve their performance. Carboxylated graphene oxide (GO-COOH) and carboxylated multiwalled carbon nanotubes (MWNT-COOH) are introduced into this sensor, because they not only have the advantages of excellent catalytic ability and a large surface area,^{24–29} but also the -COOH groups in them can be used to fix the enzyme by EDC/NHS coupling. To further enhance the electrochemical catalytic ability of the electrode, Au-Pt nanoparticles (NPs) were also deposited on the electrode, as metal NPs have a high surface/volume ratio and unusual electronic properties.^{30,31} The developed glutamate sensor is simple and practical, with the widest detection range and a lower detection limit. In addition, as the pH value of plant juice varies greatly according to different species,

different growth stages, and different tissue types, a number of working curves for the glutamate sensor were built under different pH values. Our strategy supplies a way for monitoring glutamate in vivo in a larger variety of plants and fruits.

2. MATERIALS AND METHODS

2.1. Reagents. GlutaOx, glutamate monosodium salt monohydrate, 1-(3-dimethylaminopropyl)-3-ethylcarbodiimide hydrochloride (EDC), N-hydroxysuccinimide (NHS), Nafion solution (5 wt%), bovine serum albumin (BSA), and gold(III) chloride trihydrate ($\text{HAuCl}_4 \cdot 3\text{H}_2\text{O}$) were purchased from Sigma. GO-COOH and MWNT-COOH were purchased from Xianfeng Nanomaterials Technology Co., Ltd. Chloroplatinic acid hexahydrate (H_2PtCl_6) was purchased from Macleans Biochemical Technology Co., Ltd. (Shanghai, China). Ascorbic acid, lysine, valine, aspartic acid, alanine, isoleucine, phenylalanine, leucine, glycine, and proline were purchased from Sinopharm Chemical Reagent Co., Ltd. Company (Shanghai China). The rest of the reagents are of analytical grade.

2.2. Apparatus. For studying the morphology of the modified electrode, a SEM 500 field emission scanning electron microscope system (ZEISS, Germany) was used to study the morphology of the different modified electrode, and energy-dispersive X-ray spectroscopy (EDS) which was equipped on the SEM was used to study the composition and distribution of elements of the Nafion/GlutaOx/GO-COOH-MWNT-COOH/Au-Pt/SPE sensor. All electrochemical tests are performed on an Autolab electrochemical workstation (Metrohm, Switzerland). The SPE was bought from Ningbo Mxense Biotechnology Co., Ltd. The working electrode and counter electrode are both made of carbon-based materials. The reference electrode is made of silver/

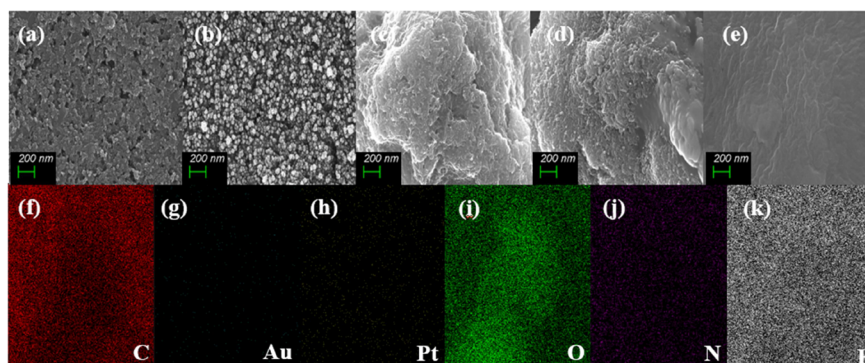


Figure 2. SEM images of bare SPE (a), Au-Pt/SPE (b), GO-COOH-MWNT-COOH/Au-Pt/SPE (c), GlutaOx/GO-COOH-MWNT-COOH/Au-Pt/SPE (d), and Nafion/GlutaOx/GO-COOH-MWNT-COOH/Au-Pt/SPE (e). (f)–(k) are the EDS mapping results for the Nafion/GlutaOx/GO-COOH-MWNT-COOH/Au-Pt/SPE.

silver chloride. All electrochemical measurements are performed at room temperature.

2.3. Nanomaterial Preparation and Electrode Fabrication. The $\text{HAuCl}_4/\text{H}_2\text{PtCl}_6$ solution was prepared by dissolving 0.081 mM HAuCl_4 and 0.160 mM H_2PtCl_6 in 0.5 mol/L H_2SO_4 . The nanocomposite of GO-COOH/MWNT-COOH was obtained by dissolving GO-COOH/MWNT-COOH (15 mg/5 mg) and EDC/NHS (10 mM/20 mM) in 10 mL DDW and subjecting it to ultrasound for 2 h. In the presence of EDC and NHS, the -COOH group in GO-COOH and MWNT-COOH can easily react with the $-\text{NH}_2$ group in GlutaOx to form amide bonds, so as to fix the enzyme. The modification process of the SPE and illustration of in vivo detection of glutamate in tomatoes are shown in Figure 1. After cleaning, the SPE was put into 5 mL of $\text{HAuCl}_4/\text{H}_2\text{PtCl}_6$ solution for electrodeposition. The $I-T$ method was used to deposit Au/Pt NPs on the SPE. The deposition voltage, time, and concentration of the $\text{HAuCl}_4/\text{H}_2\text{PtCl}_6$ solution were optimized. After washing, GO-COOH/MWNT-COOH solution of 3 μL was modified on the SPE. After dropping GO-COOH/MWNT-COOH solution three times, the electrode was dried at room temperature. Then 4 μL of BSA/GlutaOx was modified on the SPE. Finally, 2 μL of 0.5 wt% Nafion solution was added to the SPE.

3. RESULTS AND DISCUSSION

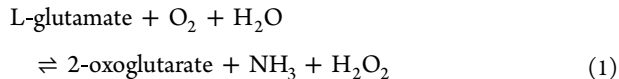
3.1. Morphology and Structure Study of the Nafion/GlutaOx/GO-COOH-MWNT-COOH/Au-Pt/SPE. Figure 2 shows the SEM characterization of electrodes. The bare SPE is shown in Figure 2a; no impurity was found on the surface of the SPE. After electrodeposition, the deposited Au/Pt NPs are densely arranged on the surface of the SPE in a regular spherical nanostructure (Figure 2b). The diameter of Au/Pt NPs is about 50–100 nm. The deposition of Au/Pt NPs will significantly increase the effective surface area and electrocatalytic performance of the SPE. When GO-COOH/MWNT-COOH was modified on the surface of the SPE (Figure 2c), tubular MWNT-COOH can be observed interspersing between layered GO-COOH. When GlutaOx was modified on the SPE surface (Figure 2d), the SPE surface became more compact and rougher. Finally, Nafion was dropped onto the SPE surface (Figure 2e), and membrane-like structures can be clearly seen. Figure 2f–k show the EDS mapping analysis results of Nafion/GlutaOx/GO-COOH-MWNT-COOH/Au-Pt/SPE, and the signals of C, Au, F, Pt,

O, and N elements are obtained. The existence of the C element is attributed to the C element in GO-COOH, MWNT-COOH, and carbon materials of the working electrode of SPE. The deposition of Au-Pt NPs accounts for the appearance of Au and Pt elements. The existence of O elements is attributed to the GlutaOx, GO-COOH, and MWNT-COOH. The existence of N elements is mainly attributed to the GlutaOx. Nafion contains F elements, which leads to the appearance of F in the EDS results. Combined with the results of SEM and EDS mapping, various materials have been confirmed to be modified successfully on the electrode surface.

3.2. Electrochemical Characterization of the Sensor Preparation Process. The modification process of the electrode was studied by cyclic voltammetry (CV) (Figure S1A). The CV test is carried out in a 5 mM $[\text{Fe}(\text{CN})_6]^{3-/4-}$ solution (containing 0.1 M KCl). Compared with the bare SPE (curve a), when Au/Pt NPs were deposited on the SPE (curve b), peak current increased significantly, indicating that the Au-Pt nanoparticles increased the conductivity of electrode. When the GO-COOH-MWNT-COOH solution was dropped on the SPE, as the conductivity of GO-COOH-MWNT-COOH is weaker compared with that of Au/Pt NPs, peak current decreased. After the modification of GlutaOx (curve d), the redox current decreased further because GlutaOx is not conductive. After the modification of Nafion (curve e), the redox peak is almost invisible. AC impedance was measured in the 0.01 Hz–100.0 kHz range (Figure S1B) and was fitted by a simple circuit. Compared to the bare SPE (curve a, $R_{ct} = 1.11 \text{ k}\Omega$), R_{ct} decreased when the electrode was modified with Au/Pt NPs (curve b, $R_{ct} = 506 \Omega$), because of the good conductivity of Au/Pt NPs. R_{ct} increased after the modification of GO-COOH-MWNT-COOH, because the conductivity of GO-COOH-MWNT-COOH was weaker compared with that of Au/Pt NPs (curve c, $R_{ct} = 733 \Omega$). After the modification of GlutaOx (curve d, $R_{ct} = 800 \Omega$) and Nafion (curve e, $R_{ct} = 10.5 \text{ k}\Omega$), R_{ct} increased further because of the insulated properties of these molecules. The CV and electrochemical impedance spectroscopy (EIS) results both confirmed the successful modification of the electrode.

3.3. Optimization of Sensor Preparation Conditions. Glutamate is nonelectroactive. The theoretical basis for development of the enzyme-based glutamate sensor is that the enzyme can oxidize glutamate, which produces a secondary electroactive product. In particular, the GlutaOx can catalyze

glutamate into α -ketoglutarate, ammonia, and H_2O_2 . H_2O_2 is then oxidized at the electrode surface. The equations of reactions are as follows:³²



Considering the great influence of potential on the sensitivity, the influence of potential on the electrochemical sensor was estimated by the I - T method. As shown in Figure S2A, by continuously adding 200 μM glutamate to 0.01 M PBS solution (pH 4.5), the effects of different applied potentials (0.5–0.9 V) on the sensor were studied. The signal-to-noise ratio (S/N) is defined as the ratio of current response signal to background noise, which can reflect the sensitivity of the detection system. It can be seen that the signal-to-noise ratio initially increases, reaches the maximum at 0.8 V, and then decreases gradually (Figure S2B). Therefore, an applied potential of 0.8 V was selected in the following experiments.

The preparation conditions of the sensor were also optimized. The optimization effects were judged according to the response current of 0.5 mM glutamate. The deposition effect of Au/Pt NPs is affected by the deposition time, so the deposition time of Au/Pt NPs was optimized. The result is shown in Figure S2C. The response current increases as the deposition time increases from 400 to 1000 s. As the deposition time continues to increase, the response current will gradually decrease. Therefore, the deposition time of 1000 s was selected as the electrodeposition time of Au/Pt NPs for the sensor.

The concentration of $\text{HAuCl}_4/\text{H}_2\text{PtCl}_6$ was optimized. The $\text{HAuCl}_4/\text{H}_2\text{PtCl}_6$ concentration of 0.016 mM/0.032 mM was used for initial electrodeposition, and then their concentrations were expanded by 5, 10, 15, and 20 times for optimization. The results are shown in Figure S2D. When the expanded time was 5, that is, the concentration ratio of $\text{HAuCl}_4/\text{H}_2\text{PtCl}_6$ is 0.081 mM/0.160 mM, the response current of glutamate is the largest, and the response current decreases with the further increase of the expanded times. Therefore, in this study, the $\text{HAuCl}_4/\text{H}_2\text{PtCl}_6$ concentration of 0.081 mM/0.160 mM was used to deposit Au/Pt NPs on the electrode.

The ratio of GO-COOH/MWNT-COOH has an important effect on the catalysis of GlutaOx. In the experiment, different ratios (4:0, 3:1, 2:2, 1:3, 0:4) of GO-COOH/MWNT-COOH on the effect of response current were investigated. From Figure S2E, when GO-COOH: MWNT-COOH is 3:1, the response current is the largest, indicating that the GO-COOH/MWNT-COOH composite material has the best synergistic effect when 3:1 is used as the ratio of GO-COOH/MWNT-COOH.

The dropping volume of GO-COOH/MWNT-COOH was also optimized. The result is shown in Figure S2F. The response current increases with the increase of volume from 3 to 9 μL , and the response current reaches the maximum at 9 μL . Therefore, 9 μL of GO-COOH/MWNT-COOH was used for the experiment.

3.4. Analytical Performance of the Glutamate Sensor.

As the pH of plant samples varies significantly, sensor performance toward glutamate may change according to different plant samples. Thus, the quantitative analysis of glutamate under different pH conditions was investigated. As

shown in Figure 3, for pH 3.5, the sensor performance is the worst. The linear range of the sensor in this pH can be divided

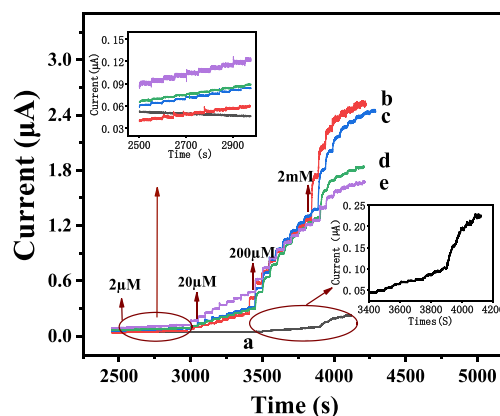


Figure 3. Representative amperometric curves of the Nafion/ GlutaOx/GO-COOH-MWNT-COOH/Au-Pt/SPE sensor for detection of different concentrations of glutamate under different pH at an applied potential of 0.8 V. (a) pH = 3.5, (b) pH = 4.5, (c) pH = 5.5, (d) pH = 6.5, and (e) pH = 7.5.

into two sections, that is, 400 μM –2 mM and 2–10 mM. The detection limit for pH 3.5 (LOD; $S/N = 3$) is 272.2 μM . For pH 4.5–7.5, the linear range of the sensor can be divided into four sections, including 2–20 μM , 20–200 μM , 200 μM –2 mM, and 2–14 mM (or 16 mM for pH 5.5). The LOD for pH 4.5, 5.5, 6.5, and 7.5 is 0.35, 0.18, 0.69, and 0.14 μM , respectively. These results indicate that the pH value of the electrolyte has a great influence on the response capacity of the sensor to glutamate, which may be caused by the deprotonation of the amide functional groups in glutamate.³³ Therefore, sensor sensitivity toward glutamate may differ as plant pH varies significantly. The detection capacity of the sensor to glutamate under pH 5.5 is the best in this range. The detailed information for the linearity and detection equations of the sensor under different pH conditions is shown in Figures S3–S7.

Figure 4 shows the current response of the sensor to glutamate at different pH values in the form of “contour”. The whole linear range is divided into four segments: 2–20 μM (Figure 4A); 20–200 μM (Figure 4B); 200 μM –2 mM (Figure 4C); 2–16 mM (Figure 4D). The corresponding glutamate concentration can be obtained intuitively through the pH value and response current. Compared to other enzymatic glutamate sensors reported previously^{22,34–41} (Table 1), the detection range of the developed glutamate sensor is widest (2 μM to 16 mM) and its detection limit is relatively low (0.14 μM). The linear range of the sensor contains the whole range of glutamate in most plants and fruits. In addition, the upper detection limit of this sensor can reach 16 mM; therefore, this sensor is suited to quantitatively detect glutamate *in vivo* in various fruits and plants.

To test the selectivity of the sensor, a variety of interferences were tested according to the approximate actual content of each amino acid in fruits (tomato was used as the model).^{21,42} The results are shown in Figure 5. The current response of interfering substances is significantly lower than that of glutamate, indicating that the developed sensor has excellent selectivity to glutamate. One fabricated glutamate sensor was tested 10 times using the same glutamate concentration

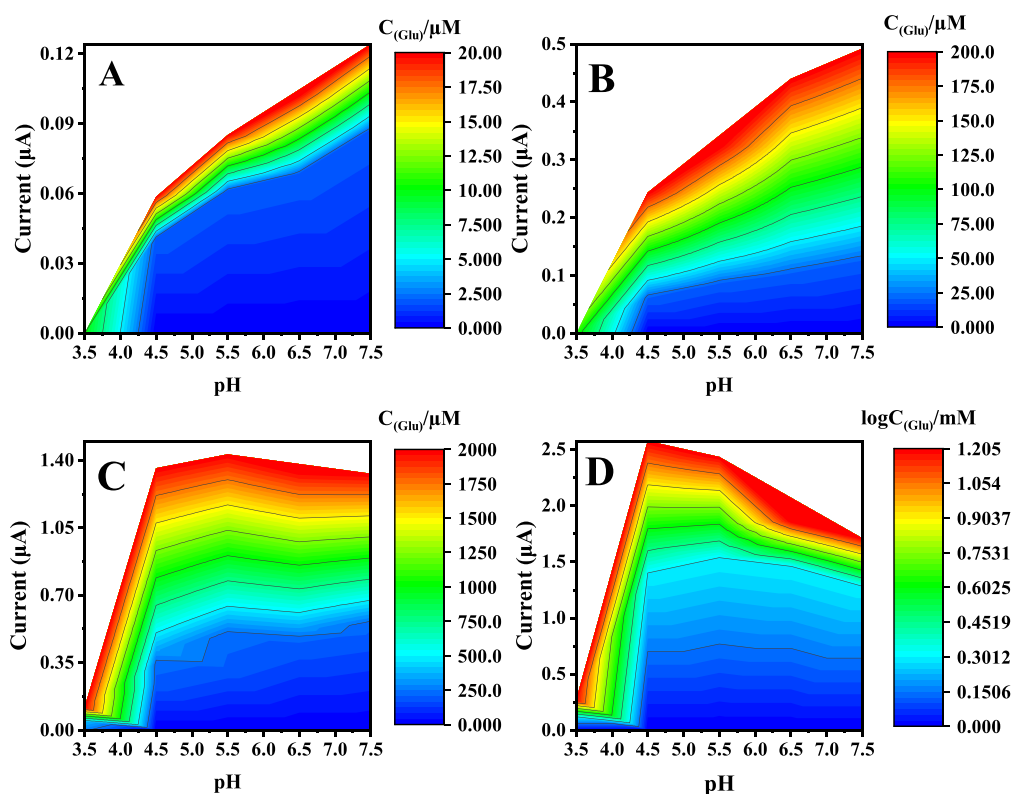


Figure 4. Step current of the Nafion/GlutaOx/GO-COOH-MWNT-COOH/Au-Pt/SPE sensor as functions of pH and glutamate concentration. (A) 2–20 μM , (B) 20–200 μM , (C) 200 μM –2 mM, and (D) 2–16 mM.

Table 1. Comparison of This Work with Various Glutamate Sensors

electrode matrix	linear range (mM)	LOD (μM)	enzyme	technique	references
$[\text{C}_3(\text{OH})_2\text{mim}][\text{BF}_4]-\text{Au}/\text{Pt}$	0.0005–0.02	0.17	GlutaOx	DPV	22
graphene/GCE	0.0001–1	0.03		DPV	34
Au/Crbxl-RGO/PtNPs	0.004–0.9	0.1	GLDH	DPV	35
Ni/Pb-core-shell	0.0001–0.5	0.052	GLDH	DPV	36
MB-SPCE	0.0125–0.15	1.5	GLDH	DPV	37
GLOx/DNA-Cu(II)/PAA/GC	0.001–0.1	1	GlutaOx	It	38
PtNPs/AuNAE	0.1–1.4	14	GlutaOx	DPV	39
Pt/ta-C/APTES/GLOx	0.01–0.5	10	GlutaOx	It	40
GLOx/silicalite/Pt	0.0025–0.45	1	GlutaOx	It	41
Nafion/GlutaOx/GO-COOH-MWNT-COOH/Au-Pt	0.002–16	0.14	GlutaOx	It	this work

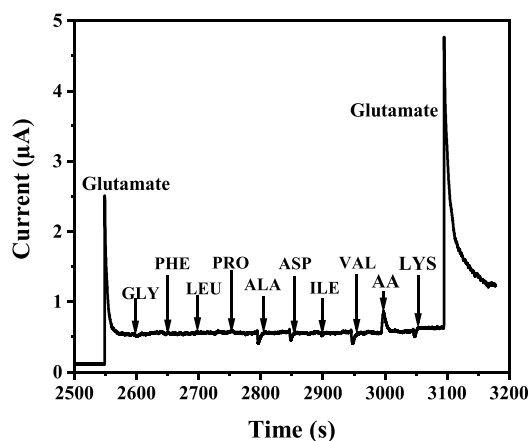


Figure 5. Selection performance test of the Nafion/GlutaOx/GO-COOH-MWNT-COOH/Au-Pt/SPE sensor.

(Figure S8A), the RSD was 4.35%. Ten glutamate sensors were also applied to test glutamate solutions of the same concentration (Figure S8B), and the RSD was 2.1%. These results indicated that the sensor has good reproducibility. After the modified electrodes were stored at 4 °C for 2 weeks, there was about 88% sensing ability remained for glutamate, indicating that the modified electrodes were highly stable.

3.5. Practical Detection of Glutamate in Tomatoes.

To test the prospect of the sensor in detecting practical samples, a standard addition method was used. As shown in Table S1, the recovery of glutamate in the tomato samples was in the range of 99.4–108.7% ($n = 5$), which suggested that the sensor is accurate and reliable.

Considering the impedance difference of glutamate standard solution, tomato juice, and tomato fruit, EIS and the impedance time technique were used to test the impedance of glutamate standard solution, 100% tomato juice, and tomato fruit (Figure 6A/B). The results showed that the R_{ct} of tomato juice (1207 Ω) was close to that of glutamate standard solution

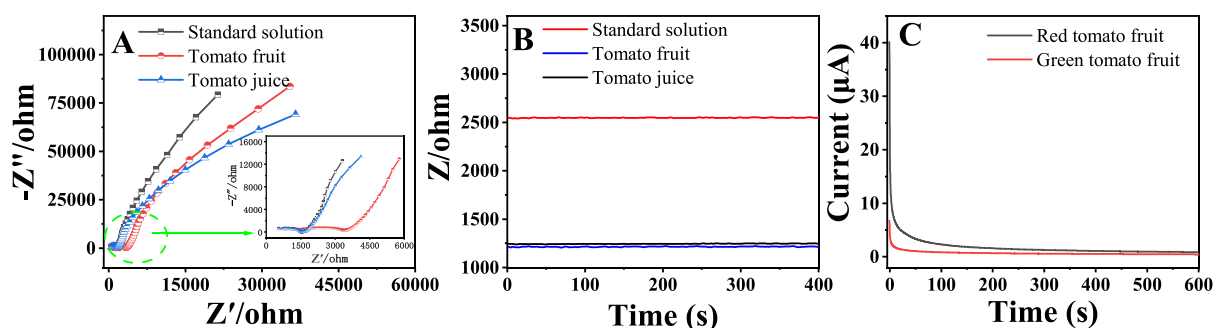


Figure 6. EIS diagram (A) and impedance time diagram (B) of the tomato fruit, tomato juice, and glutamate solution. (C) I – T curve of glutamate in red and green tomatoes in tomato plants.

(1242 Ω), but the R_{ct} value of tomato fruits reached 2550 Ω , which was about twice that of tomato juice. Using the heterogeneous charge-transfer resistance as a correction index, a similar current response of glutamate can be obtained in tomatoes (0.75 μA) and tomato juice (0.77 μA). Thus, the following equation is proposed to calibrate the glutamate in tomatoes

$$I = \frac{Z_{\text{fruit}}}{Z_{\text{Glu solution}}} \times I_{\text{fruit}}$$

In this equation, I and I_{fruit} are the response current for glutamate in glutamate solution and tomato fruit, and $Z_{\text{Glu solution}}$ and Z_{fruit} are the R_{ct} values of glutamate solution and tomato fruit. Then the real glutamate content in tomato fruits can be obtained after substituting the corrected I into the linear regression equation.

The constructed glutamate sensor was used to detect glutamate in different growth stages of tomatoes. The glutamate level was monitored in situ by inserting the sensor directly into the tomato. After inserting, the I – T current response quickly reaches a steady state (about 500 s). The I – T curves of glutamate in green and red fruits are shown in Figure 6C. The corresponding impedance results of red tomato and green tomato were shown in Figure S9. Using the equation mentioned above, the current responses of the green (pH = 4.0) and red tomato fruits (pH = 4.5) are 0.51 and 0.96 μA , which correspond to the glutamate concentration of 1298 and 1375 μM according to the step current model. This result is roughly the same as the glutamate content in tomatoes reported in previous research,⁴³ indicating that the glutamate content in tomato fruits increases significantly during tomato fruit ripening. These results may be related to the high protein turnover rate of the ripening stage. These results also indicated that the sensor can be used to in situ monitor the glutamate level in fruits.

4. CONCLUSIONS

In this work, a new amperometric glutamate sensor based on the Nafion/GlutaOx/GO–COOH–MWNT–COOH/Au–Pt/SPE was developed. Compared with the glutamate sensors reported previously, the detection range of our fabricated glutamate sensor is widest, which contains the whole concentration range of glutamate in varieties of fruits and plants. Its application for in vivo monitoring of glutamate content in tomatoes was also demonstrated. In addition, as the pH value of plant juice varies greatly, a number of working curves for the glutamate sensor were built at different pH values, which can be applied for determining glutamate in vivo

in varieties of fruits and plants. The glutamate sensor has important applied value in precision agriculture. Our strategy also provides a way to establish the detection modes for other biomolecules.

■ ASSOCIATED CONTENT

Supporting Information

The Supporting Information is available free of charge at <https://pubs.acs.org/doi/10.1021/acsomega.2c04029>.

CV and EIS plots of the modification process of the electrode; details of optimization of preparation conditions of the sensor; details of the linearity and detection equations of the sensor under different pH conditions; details of the reproducibility test of the sensor; EIS diagram and impedance time diagram of the red and green tomatoes in tomato plants; and details of recovery of glutamate in the tomato samples (PDF)

■ AUTHOR INFORMATION

Corresponding Author

Aixue Li – Research Center of Intelligent Equipment, Beijing Academy of Agriculture and Forestry Sciences, Beijing 100097, China; orcid.org/0000-0001-6476-3005; Email: aixueli_2021@163.com, liax@nercita.org.cn

Authors

Shunkun Tang – Research Center of Intelligent Equipment, Beijing Academy of Agriculture and Forestry Sciences, Beijing 100097, China; College of Landscape and Ecological Engineering, Hebei University of Engineering, Handan 056038, China

Cheng Wang – Research Center of Intelligent Equipment, Beijing Academy of Agriculture and Forestry Sciences, Beijing 100097, China

Ke Liu – Research Center of Intelligent Equipment, Beijing Academy of Agriculture and Forestry Sciences, Beijing 100097, China

Bin Luo – Research Center of Intelligent Equipment, Beijing Academy of Agriculture and Forestry Sciences, Beijing 100097, China

Hongtu Dong – Research Center of Intelligent Equipment, Beijing Academy of Agriculture and Forestry Sciences, Beijing 100097, China

Xiaodong Wang – Research Center of Intelligent Equipment, Beijing Academy of Agriculture and Forestry Sciences, Beijing 100097, China

Peichen Hou – Research Center of Intelligent Equipment,
Beijing Academy of Agriculture and Forestry Sciences, Beijing
100097, China

Complete contact information is available at:
<https://pubs.acs.org/10.1021/acsomega.2c04029>

Author Contributions

S.T. and C.W. performed the experiments, analyzed the data, and wrote the original manuscript. K.L., B.L., H.D., X.W., and P.H. helped to perform the experiments. A.L. supervised the project, designed the research, wrote-reviewed, and edited the manuscript. All authors contributed to the article and approved the submitted version. S.T. and C.W. contributed equally to this work.

Notes

The authors declare no competing financial interest.

ACKNOWLEDGMENTS

The authors are thankful for the fundings from the National Natural Science Foundation of China (Grant No. 21974012), Beijing Natural Science Foundation (2222007), and Key-Area Research and Development Program of Guang Dong Province (No. 2021B0707010002).

REFERENCES

- (1) Seifi, H. S.; Van Bockhaven, J.; Angenon, G.; Höfte, M. Glutamate metabolism in plant disease and defense: friend or foe? *Mol. Plant-Microbe Interact.* **2013**, *26*, 475–485.
- (2) Galili, G.; Tang, G.; Zhu, X.; Gakiere, B. Lysine catabolism: a stress and development super-regulated metabolic pathway. *Curr. Opin. Plant Biol.* **2001**, *4*, 261–266.
- (3) Fait, A.; Fromm, H.; Walter, D.; Galili, G.; Fernie, A. R. Highway or byway: the metabolic role of the GABA shunt in plants. *Trends Plant Sci.* **2008**, *13*, 14–19.
- (4) Shelp, B. J.; Bozzo, G. G.; Trobacher, C. P.; Zarei, A.; Deyman, K. L.; Brikis, C. J. Hypothesis/review: contribution of putrescine to 4-aminobutyrate (GABA) production in response to abiotic stress. *Plant Sci.* **2012**, *193*, 130–135.
- (5) Forde, B. G.; Lea, P. J. Glutamate in plants: metabolism, regulation, and signalling. *J. Exp. Bot.* **2007**, *58*, 2339–2358.
- (6) Monge-Acuña, A. A.; Fornaguera-Trías, J. A high performance liquid chromatography method with electrochemical detection of gamma-aminobutyric acid, glutamate and glutamine in rat brain homogenates. *J. Neurosci. Methods* **2009**, *183*, 176–181.
- (7) Buck, K.; Voehringer, P.; Ferger, B. Rapid analysis of GABA and glutamate in microdialysis samples using high performance liquid chromatography and tandem mass spectrometry. *J. Neurosci. Methods* **2009**, *182*, 78–84.
- (8) Tang, L.; Zhu, Y.; Xu, L.; Yang, X.; Li, C. Amperometric glutamate biosensor based on self-assembling glutamate dehydrogenase and dendrimer-encapsulated platinum nanoparticles onto carbon nanotubes. *Talanta* **2007**, *73*, 438–443.
- (9) Acebal, C. C.; Lista, A. G.; Band, B. S. F. Simultaneous determination of flavor enhancers in stock cube samples by using spectrophotometric data and multivariate calibration. *Food Chem.* **2008**, *106*, 811–815.
- (10) Tsukatani, T.; Matsumoto, K. Sequential fluorometric quantification of γ -aminobutyrate and l-glutamate using a single line flow-injection system with immobilized-enzyme reactors. *Anal. Chim. Acta* **2005**, *546*, 154–160.
- (11) Chakraborty, S.; Raj, C. R. Amperometric biosensing of glutamate using carbon nanotube based electrode. *Electrochem. Commun.* **2007**, *9*, 1323–1330.
- (12) Cserhádi, T. Chromatography of amino acids and short peptides. New advances. *Biomed. Chromatogr.* **2007**, *21*, 780–796.
- (13) Fan, J.; Qi, K.; Zhang, L.; Zhang, H.; Yu, S.; Cui, X. Engineering Pt/Pd interfacial electronic structures for highly efficient hydrogen evolution and alcohol oxidation. *ACS Appl. Mater. Interfaces* **2017**, *9*, 18008–18014.
- (14) Guo, J. Smartphone-powered electrochemical dongle for point-of-care monitoring of blood β -ketone. *Anal. Chem.* **2017**, *89*, 8609–8613.
- (15) Sun, X.; Hui, N.; Luo, X. Reagentless and label-free voltammetric immunosensor for carcinoembryonic antigen based on polyaniline nanowires grown on porous conducting polymer composite. *Microchim. Acta* **2017**, *184*, 889–896.
- (16) Riberi, W. I.; Tarditto, L. V.; Zon, M. A.; Arévalo, F. J.; Fernández, H. Development of an electrochemical immunosensor to determine zeaxanthone in maize using carbon screen printed electrodes modified with multi-walled carbon nanotubes/polyethyleneimine dispersions. *Sens. Actuators, B* **2018**, *254*, 1271–1277.
- (17) Serafín, V.; Valverde, A.; Martínez-García, G.; Martínez-Perián, E.; Comba, F.; Garranzo-Asensio, M.; Barderas, R.; Yáñez-Sedeño, P.; Campuzano, S.; Pingarrón, J. Graphene quantum dots-functionalized multi-walled carbon nanotubes as nanocarriers in electrochemical immunosensing. Determination of IL-13 receptor $\alpha 2$ in colorectal cells and tumor tissues with different metastatic potential. *Sens. Actuators, B* **2019**, *284*, 711–722.
- (18) Doménech-Carbó, A.; Dias, D.; Donnici, M. In vivo Electrochemical Monitoring of Signaling Transduction of Plant Defense Against Stress in Leaves of Aloe vera L. *Electroanalysis* **2021**, *33*, 1024–1032.
- (19) Nguyen, T. N.; Nolan, J. K.; Park, H.; Lam, S.; Fattah, M.; Page, J. C.; Joe, H.-E.; Jun, M. B.; Lee, H.; Kim, S. J. Facile fabrication of flexible glutamate biosensor using direct writing of platinum nanoparticle-based nanocomposite ink. *Biosens. Bioelectron.* **2019**, *131*, 257–266.
- (20) Ganesana, M.; Triantopoulou, E.; Maniar, Y.; Lee, S. T.; Venton, B. J. Development of a novel micro biosensor for in vivo monitoring of glutamate release in the brain. *Biosens. Bioelectron.* **2019**, *130*, 103–109.
- (21) Huang, Y. Determination of free amino acids in common fruits and vegetables. *J. Anhui Agric. Sci.* **2013**, *41*, 4088–4089.
- (22) Yu, Y.; Liu, X.; Jiang, D.; Sun, Q.; Zhou, T.; Zhu, M.; Jin, L.; Shi, G. [C₃(OH)₂mim][BF₄]-Au/Pt biosensor for glutamate sensing in vivo integrated with on-line microdialysis system. *Biosens. Bioelectron.* **2011**, *26*, 3227–3232.
- (23) Doaga, R.; McCormac, T.; Dempsey, E. Electrochemical Sensing of NADH and Glutamate Based on Meldola Blue in 1,2-Diaminobenzene and 3,4-Ethylenedioxythiophene Polymer Films. *Electroanalysis* **2009**, *21*, 2099–2108.
- (24) Mani, V.; Chen, S.-M.; Lou, B.-S. Three dimensional graphene oxide-carbon nanotubes and graphene-carbon nanotubes hybrids. *Int. J. Electrochem. Sci.* **2013**, *8*, 11641–11660.
- (25) Gao, W.; Tjiu, W. W.; Wei, J.; Liu, T. Highly sensitive nonenzymatic glucose and H₂O₂ sensor based on Ni(OH)₂/electroreduced graphene oxide–Multiwalled carbon nanotube film modified glass carbon electrode. *Talanta* **2014**, *120*, 484–490.
- (26) Gulati, P.; Kaur, P.; Rajam, M.; Srivastava, T.; Mishra, P.; Islam, S. Vertically aligned multi-walled carbon nanotubes based flexible immunosensor for extreme low level detection of multidrug resistant leukemia cells. *Sens. Actuators, B* **2019**, *301*, No. 127047.
- (27) Kamran, U.; Heo, Y.-J.; Lee, J. W.; Park, S.-J. Functionalized carbon materials for electronic devices: a review. *Micromachines* **2019**, *10*, 234.
- (28) Li, X.; Ping, J.; Ying, Y. Recent developments in carbon nanomaterial-enabled electrochemical sensors for nitrite detection. *TrAC, Trends Anal. Chem.* **2019**, *113*, 1–12.
- (29) Hernaez, M. Applications of Graphene-Based Materials in Sensors. *Sensors* **2020**, *20*, 3196.
- (30) Tian, Y.; Liu, H.; Zhao, G.; Tatsuma, T. Shape-controlled electrodeposition of gold nanostructures. *J. Phys. Chem. B* **2006**, *110*, 23478–23481.

(31) Daniel, M.-C.; Astruc, D. Gold nanoparticles: assembly, supramolecular chemistry, quantum-size-related properties, and applications toward biology, catalysis, and nanotechnology. *Chem. Rev.* **2004**, *104*, 293–346.

(32) Scoggin, J. L.; Tan, C.; Nguyen, N. H.; Kansakar, U.; Madadi, M.; Siddiqui, S.; Arumugam, P. U.; DeCoster, M. A.; Murray, T. A. An enzyme-based electrochemical biosensor probe with sensitivity to detect astrocytic versus glioma uptake of glutamate in real time in vitro. *Biosens. Bioelectron.* **2019**, *126*, 751–757.

(33) Pshenichnyuk, S. A.; Modelli, A.; Jones, D.; Lazneva, E. F.; Komolov, A. S. Low-energy electron interaction with melatonin and related compounds. *J. Phys. Chem. B* **2017**, *121*, 3965–3974.

(34) Kang, H.; Jin, Y.; Han, Q. Electrochemical detection of epinephrine using an L-glutamic acid functionalized graphene modified electrode. *Anal. Lett.* **2014**, *47*, 1552–1563.

(35) Barman, S. C.; Hossain, M.; Yoon, H.; Park, J. Y. Carboxyl terminated reduced graphene oxide (Crbxl-RGO) and Pt nanoparticles based ultra-sensitive and selective electrochemical biosensor for glutamate detection. *J. Electrochem. Soc.* **2018**, *165*, B296.

(36) Yu, H.; Ma, Z.; Wu, Z. Immobilization of Ni–Pd/core–shell nanoparticles through thermal polymerization of acrylamide on glassy carbon electrode for highly stable and sensitive glutamate detection. *Anal. Chim. Acta* **2015**, *896*, 137–142.

(37) Hughes, G.; Pemberton, R.; Fielden, P.; Hart, J. P. Development of a novel reagentless, screen-printed amperometric biosensor based on glutamate dehydrogenase and NAD⁺, integrated with multi-walled carbon nanotubes for the determination of glutamate in food and clinical applications. *Sens. Actuators, B* **2015**, *216*, 614–621.

(38) Hasebe, Y.; Gu, T.; Kusakabe, H. Glutamate biosensor using a DNA–Cu (II)/polyamine membrane as a novel electrocatalytic layer for cathodic determination of hydrogen peroxide. *Electrochemistry* **2006**, *74*, 179–182.

(39) Jamal, M.; Xu, J.; Razeeb, K. M. Disposable biosensor based on immobilisation of glutamate oxidase on Pt nanoparticles modified Au nanowire array electrode. *Biosens. Bioelectron.* **2010**, *26*, 1420–1424.

(40) Kaivosoja, E.; Tujunen, N.; Jokinen, V.; Protopopova, V.; Heinilä, S.; Koskinen, J.; Laurila, T. Glutamate detection by amino functionalized tetrahedral amorphous carbon surfaces. *Talanta* **2015**, *141*, 175–181.

(41) Soldatkina, O.; Soldatkin, O.; Kasap, B. O.; Kucherenko, D. Y.; Kucherenko, I.; Kurc, B. A.; Dzyadevych, S. A novel amperometric glutamate biosensor based on glutamate oxidase adsorbed on silicalite. *Nanoscale Res. Lett.* **2017**, *12*, 1–8.

(42) Ferraro, G.; D'Angelo, M.; Sulpice, R.; Stitt, M.; Valle, E. M. Reduced levels of NADH-dependent glutamate dehydrogenase decrease the glutamate content of ripe tomato fruit but have no effect on green fruit or leaves. *J. Exp. Bot.* **2015**, *66*, 3381–3389. (accessed 7/26/2022)

(43) Sorregheta, A.; Ferraro, G.; Boggio, S. B.; Valle, E. M. Free amino acid production during tomato fruit ripening: a focus on L-glutamate. *Amino Acids* **2010**, *38*, 1523–1532.